QUADRATURE RULE FOR SOLVING THE HELMHOLTZ EQUATION IN HYPERSINGULAR BEM FORMULATION

ANTONIO ROMERO[1], ROCIO VELÁZQUEZ-MATA[1], JOSE DOMÍNGUEZ[1],
ANTONIO TADEU[2,3] & PEDRO GALVÍN[1,4]
[1]Escuela Técnica Superior de Ingeniería, Universidad de Sevilla, Spain
[2]University of Coimbra, CERIS, Department of Civil Engineering, Portugal
[3]Itecons, Institute of Research and Technological Development in Construction, Energy,
Environment and Sustainability, Portugal
[4]ENGREEN, Laboratory of Engineering for Energy and Environmental Sustainability,
Universidad de Sevilla, Spain

ABSTRACT

Velázquez-Mata et al. [1] recently presented a quadrature rule to accurately evaluate singular and weakly singular integrals in the sense of the Cauchy Principal Value by an exclusively numerical procedure. The procedure was verified by solving engineering problems using the boundary element method with fundamental solutions that have singularities of type $\log(r)$ and $1/r$. However, that quadrature does not handle the evaluation of the Hadamard Finite Part of hypersingular integrals. These types of singularity appear in several fundamental solutions and, also, when the hypersingular boundary element formulation is applied to the Green functions previously analysed by the authors. In this paper, the quadrature rule presented in Velázquez-Mata et al. [1] is extended to accurately compute integrals with singularities of the type $1/r^2$. The quadrature weights are derived from a system of equations defined from the finite part of known integrals called generalised moments, which include the element shape functions. This novelty is included in the hypersingular formulation of the boundary element method to solve the Helmholtz equation, taking advantage of this methodology to consider null-thickness boundaries using the Dual BEM.

Keywords: hypersingular formulation, dual BEM, boundary integral equation, hypersingular kernels, singular kernels, Bézier curve.

1 INTRODUCTION

The formulation of the classical boundary element method (BEM) results in boundary integral equations (BIE) for a point $\mathbf{x}^*$ located at the arbitrary boundary Γ as follows [2]:

$$c(\mathbf{x}^*)u(\mathbf{x}^*) = \int_\Gamma \left(t(\mathbf{x})\mathcal{G}(\mathbf{x},\mathbf{x}^*) - u(\mathbf{x})\mathcal{H}(\mathbf{x},\mathbf{x}^*)\right)\,d\Gamma(\mathbf{x}), \qquad (1)$$

where $u(\mathbf{x})$ and $t(\mathbf{x})$ are the field variables, $\mathcal{G}(\mathbf{x},\mathbf{x}^*)$ and $\mathcal{H}(\mathbf{x},\mathbf{x}^*)$ are the fundamental solution at the point $\mathbf{x}$ due to a point source located at $\mathbf{x}^*$, and the integral-free term $c(\mathbf{x}^*)$ depends only on the boundary geometry at the collocation point $\mathbf{x}^*$.

The hypersingular formulation is much better suited for some applications, such as when minimal thickness should be modelled. The hypersingular boundary element formulation or the traction boundary element method (TBEM) is obtained by taking the boundary integral gradient in eqn (1):

$$c(\mathbf{x}^*)t(\mathbf{x}^*) + a(\mathbf{x}^*)u(\mathbf{x}^*) = \int_\Gamma (t(\mathbf{x})\tilde{\mathcal{G}}(\mathbf{x},\mathbf{x}^*) - u(\mathbf{x})\tilde{\mathcal{H}}(\mathbf{x},\mathbf{x}^*))\,d\Gamma(\mathbf{x}), \qquad (2)$$

where the coefficients $a(\mathbf{x}^*)$ are zeros in the cases indicated by Guiggiani [3] that include the ones considered in this paper, and $\tilde{\mathcal{G}}(\mathbf{x},\mathbf{x}^*)$ and $\tilde{\mathcal{H}}(\mathbf{x}$ and $\mathbf{x}^*)$ are obtained from the derivatives of the fundamental solution.

The integrals in eqns (1) and (2) can be regular, near-singular, weakly singular, singular, or hypersingular integrals and should be understood in the sense of the Cauchy Principal Value (CPV) or in the Hadamard Finite Part (FP). It should be indicated that the order of the singularity increases in the hypersingular formulation as the gradient is taken. This work extends the quadrature rule presented in Velázquez-Mata et al. [1] to the hypersingular BEM formulation, enabling an accurate computation of integrals with higher order singularities.

The paper is organised as follows. First, the hypersingular BEM formulation is briefly described, and the numerical quadrature is developed to consider singularities of type $1/r^2$ by evaluating the corresponding generalised moment. Then, the proposed methodology is numerically verified by solving the Helmholtz equation on an open boundary. Dirichlet and Neumann boundary conditions are both prescribed, and the results computed by the classical and hypersingular BEM formulations are compared. Second, an illustration of the applicability of the proposed technique for solving the Helmholtz equation in domains with inclusions is presented. The BEM and TBEM formulations are both coupled to represent null-thickness boundaries. Finally, the main results of this research are summarised.

2   BEM FORMULATIONS

The starting point for the BEM formulation is the BIE (eqn (1)). Once the boundary is discretised into N elements, $\Gamma = \bigcup_{j=1}^{N} \Gamma^j$, and the field variables within an element Γ^j are approximated from the nodal values u^i and t^i through the element shape functions $\phi^i(\mathbf{x})$ of order p, the eqn (1) is rewritten as follows:

$$c(\mathbf{x}^*)u(\mathbf{x}^*) = \sum_{j=1}^{N}\sum_{i=0}^{p}\left[\left(\int_{\Gamma^j}\phi^i(\mathbf{x})\mathcal{G}(\mathbf{x},\mathbf{x}^*)\,d\Gamma\right)t^i - \left(\int_{\Gamma^j}\phi^i(\mathbf{x})\mathcal{H}(\mathbf{x},\mathbf{x}^*)\,d\Gamma\right)u^i\right] \quad (3)$$

Similarly, the hypersingular form of the BIE (eqn (2)) leads to the following expression after boundary discretisation:

$$c(\mathbf{x}^*)t(\mathbf{x}^*) = \sum_{j=1}^{N}\sum_{i=0}^{p}\left[\left(\int_{\Gamma^j}\phi^i(\mathbf{x})\tilde{\mathcal{G}}(\mathbf{x},\mathbf{x}^*)\,d\Gamma\right)t^i - \left(\int_{\Gamma^j}\phi^i(\mathbf{x})\tilde{\mathcal{H}}(\mathbf{x},\mathbf{x}^*)\,d\Gamma\right)u^i\right] \quad (4)$$

Eqns (3) and (4), can be coupled to produce the Dual BEM formulation, as will be done in Section 4.

A critical step in the BEM formulation is the integration of elements, as mentioned above. The integral kernel usually has a singularity that depends on the physical problem. Moreover, the kernels of the hypersingular formulation are strongly singular. Typically, these singularities are of the form $\log(r)$, $1/r$ and $1/r^2$. The element integration should then be computed according to the singularity but also to the element order p used for the field approximation.

It was shown in Romero et al. [4] that the element shape functions $\phi^i(\mathbf{x})$ of order p based on a Lagrange interpolant can be derived from the Bernstein basis as:

$$\phi^i(t) = \sum_{k=0}^{n} c_k^i B_k^n(t), \quad i = 0,\ldots,p \quad (5)$$

where c_k^i are control points and $B_k^n(t)$ is the Bernstein polynomial of order n defined over the interval $t \in [0,1]$:

$$B_k^n(t) = \binom{n}{k}t^k(1-t)^{n-k}, \quad k = 0,\ldots,n \quad (6)$$

The Lagrange interpolant must fulfil $\phi^i(t_j) = \sum_{k=0}^{n} c_k^i B_k^n(t_j) = \delta_{ij}$, $j = 0, \ldots, n$ at the element nodes t_j, where δ_{ij} is the Kronecker delta. This condition is commonly expressed as a linear system of equations through the Bernstein–Vandermonde matrix $A_{jk} = B_k^n(t_j)$.

Once the control points c_k^i are obtained, the element integration in eqns (3) and (4) can be rewritten as follows in the natural coordinate ξ according to eqn (5):

$$
\begin{aligned}
\int_{-1}^{1} \phi^i(\xi) \mathcal{F}(\xi, \mathbf{x}^*) \frac{d\Gamma}{d\xi} \, d\xi &= \int_{0}^{1} \phi^i(t) \mathcal{F}(t, \mathbf{x}^*) \frac{d\Gamma}{d\xi} \frac{d\xi}{dt} \, dt \\
&= \int_{0}^{1} \left(\sum_{k=0}^{n} c_k^i B_k^n(t) \right) \mathcal{F}(t, \mathbf{x}^*) \frac{d\Gamma}{d\xi} \frac{d\xi}{dt} \, dt \qquad (7) \\
&= \sum_{k=0}^{n} c_k^i \left(\int_{0}^{1} B_k^n(t) \mathcal{F}(t, \mathbf{x}^*) \frac{d\Gamma}{d\xi} \frac{d\xi}{dt} \, dt \right)
\end{aligned}
$$

where, $\mathcal{F}(t, \mathbf{x}^*)$ stands for the type of singularity in the fundamental solution.

The quadrature rule presented by the authors in Velázquez-Mata et al. [1] is extended in this work to assess hypersingular kernels, as well as weakly singular and singular integrations. The proposed quadrature allows us to evaluate the BIE numerically for any element order p.

3 QUADRATURE RULES

The quadrature rules proposed here are based on the recent work published by Velázquez-Mata et al. [1]. However, one of the novelties of this paper is to develop a numerical quadratures so that integrals with singularities of the type $1/r^2$ can be computed without loss of accuracy in the estimation of weakly singular and singular integrals. Thus, the quadrature rule enable the calculation of eqn (7) accounting for $\mathcal{F}(\xi, \mathbf{x}^*)$ equals 1, $\log |\xi^* - \xi|$, $(\xi^* - \xi)^{-1}$ and $(\xi^* - \xi)^{-2}$, where ξ^* is the natural coordinate of the collocation point at the integration element.

The quadrature of order M should approximate the integrals in eqn (7) as:

$$
\int_{-1}^{1} B_k^n(\xi) \mathcal{F}(\xi, \mathbf{x}^*) \, d\xi = \int_{0}^{1} B_k^n(t) \mathcal{F}(t, \mathbf{x}^*) \frac{d\xi}{dt} \, dt \simeq \sum_{m=0}^{M} B_k^n(t_m) \mathcal{F}(t_m, \mathbf{x}^*) \frac{d\xi}{dt} w_m \quad (8)
$$

where t_m and w_m are the integration points and weights, respectively. Quadrature weights are obtained from the solution of a system of equations defined from the above approximation [1]:

$$
\sum_{m=0}^{M} \psi_k(t_m, \xi^*) w_m = m_k, \qquad k = 0, \ldots, n \qquad (9)
$$

where $\psi_k(t_m, \xi^*) = B_k^n(t) \mathcal{F}(t_m, \mathbf{x}^*) d\xi/dt$ stands for the integral kernel and m_k represents the generalised moment, that is, the exact solution of eqn (8). The generalised moments can be obtained from the Brandaõ approach to the finite part integrals [5] according to Carley [6]. The solution of the generalised moment for weakly singular and singular integrals can be found in Velázquez-Mata et al. [1].

The following generalised moment should be included in the methodology for integrating hypersingular kernels:

$$
m_k = \text{FP} \int_{-1}^{1} \frac{B_k^n(\xi)}{(\xi^* - \xi)^2} \, d\xi = \text{FP} \int_{0}^{1} \frac{B_k^n(t)}{(\xi^* - 2t + 1)^2} \frac{d\xi}{dt} \, dt \qquad (10)
$$

In addition to the generalised moment proposed in Velázquez-Mata et al. [1], the solution of the generalised moment expressed on the univariate basis $t \in [0, 1]$ is obtained according to the following formulas [5], [6]:

$$
\begin{aligned}
m_k &= \text{FP} \int_0^1 \frac{B_k^n(t)}{(\xi^* - 2t + 1)^2} \frac{d\xi}{dt} \, dt \\
&= B_k^n(t^*) \text{FP} \int_0^1 \frac{1}{(\xi^* - 2t + 1)^2} \frac{d\xi}{dt} \, dt - \frac{dB_k^n(t^*)}{dt} \frac{dt}{d\xi} \text{CPV} \int_0^1 \frac{1}{\xi^* - 2t + 1} \frac{d\xi}{dt} \, dt \quad (11) \\
&\quad + \int_0^1 \frac{B_k^n(t) - B_k^n(t^*) + \dfrac{dB_k^n(t^*)}{dt} \dfrac{dt}{d\xi}(\xi^* - 2t + 1)}{\xi^* - 2t + 1} \frac{d\xi}{dt} \, dt
\end{aligned}
$$

where

$$
\text{FP} \int_0^1 \frac{1}{(\xi^* - 2t + 1)^2} \frac{d\xi}{dt} \, dt = \begin{cases} 2/(\xi^{*2} - 1) & |\xi^*| \neq 1 \\ -1/2 & \xi^* = \pm 1 \end{cases} \quad (12)
$$

$$
\text{CPV} \int_0^1 \frac{1}{\xi^* - 2t + 1} \frac{d\xi}{dt} \, dt = \begin{cases} \log \left| \dfrac{\xi^* + 1}{1 - \xi^*} \right| & |\xi^*| \neq 1 \\ \pm \log(2) & \xi^* = \pm 1 \end{cases} \quad (13)
$$

Then, the system of eqn (9) includes $n + 1$ equations for each type of function to be integrated. The quadrature rule proposed in this work is capable of integrating kernels with constant, $\log(r)$, $1/r$, and $1/r^2$ terms when the collocation point belongs to the integration element, which are found in the fundamental solution or in their series expansions. Therefore, eqn (9) defines a system of $4(n + 1)$ equations with $M + 1$ unknown weights w_m. The solution is obtained in the least-squares sense when overdetermined and in the minimum norm least-squares sense when undetermined. The integration point should not be located at the natural coordinates of the collocation nodes to avoid indeterminate terms in eqn (9).

3.1 Numerical validation

Table 1 summarises the integral values calculated from FP $\int_{-1}^1 \phi^i (\xi - \xi^*)^{-2} \, d\xi$ for the five shape functions corresponding to the Chebyshev points of the first kind, of order $p = 4$ and $\xi^* = 0$. This integrand presents a singularity at $\xi = 0$ for the shape function $i = 2$ with nonzero value at ξ^*. The integral is numerically evaluated using the proposed approach and using the built-in MATLAB function integral [7] for comparison purposes, and both solutions are compared with the exact values computed from eqns (7) and (11). The integral is only correctly evaluated when the proposed methodology is used.

Fig. 1 shows the L_2 scaled error ϵ_2 in the integral computation in eqn (10) for different element order and point distributions: (i) Chebyshev points of the first kind; (ii) Chebyshev points of the second kind; (iii) LGL integration points; and (iv) equidistant nodes [4]. The accuracy of the proposed quadrature rules is analysed for different numbers of integration points M according to the shape function of order p. The quadrature rule gave errors lower than $\mathcal{O}(10^{-5})$ in all cases. The integration error increases with the element order p, and is slightly affected by the number of integration points for $M \geq 4(p + 1)$. Therefore, a value for M equal to $4(p + 1)$ is considered, as in Velázquez-Mata et al. [1] for singularities of types $\log(r)$ and $1/r$.

Moreover, an additional test was performed as that presented in Guiggiani and Casalini [8] by Guiggiani and Casalini to calculate the finite part of the function $g(x) = (x^3 + 1)/x^2$. Two

Table 1: Computed integral values of FP $\int_{-1}^{1} \phi^i (\xi - \xi^*)^{-2} \, d\xi$ for shape function ϕ^i of order $p = 4$ defined at Chebyshev points of the first kind and $\xi^* = 0$: (i) evaluated by the proposed approach (Q), (ii) using the built-in `integral` MATLAB function (I), and (iii) exact values (eqns (7) and (11)) (M). The values corresponding to the shape function that presents a non-zero value at $\xi = \xi^*$ are highlighted in grey.

i	M	Q	I
0	-0.024045	-0.024045	-0.023959
1	2.957379	2.957379	2.957178
2	-7.866667	-7.866667	312551427532.072510
3	2.957379	2.957379	2.957332
4	-0.024045	-0.024045	-0.024059
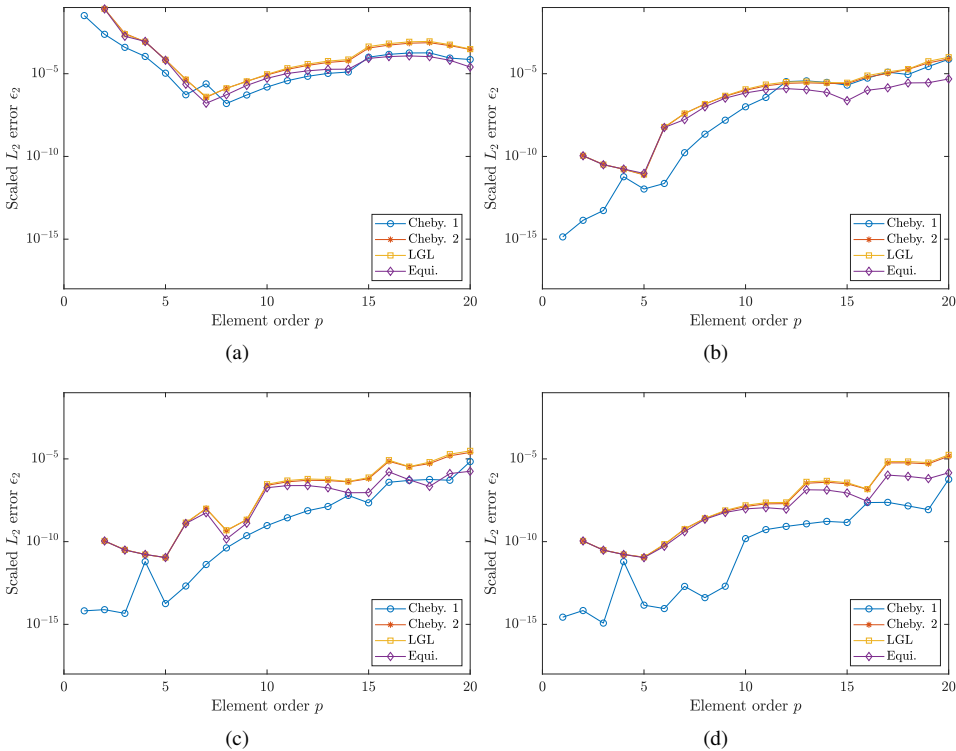
Figure 1: L_2 scaled error ϵ_2 in the computation of the integral in eqn (10) using (a) $M = 2(p+1)$; (b) $M = 3(p+1)$; (c) $M = 4(p+1)$; and (d) $M = 8(p+1)$ integration points.
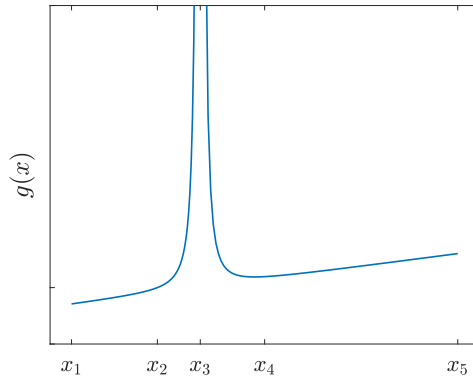
Figure 2: Test on the integration procedure.

quadratic elements $\Gamma^a := [x_1, x_2, x_3]$ and $\Gamma^b := [x_3, x_4, x_5]$ were used to integrate. The test consists of the calculation of the finite part given by:

$$\text{FP} \int_{x_2}^{x_4} \frac{x^3 + 1}{x^2} dx \tag{14}$$

The integrand has singularity at $x = 0$ of order $1/r^2$ (see Fig. 2). The exact value of the finite part is [9]:

$$\text{FP} \int_{x_2}^{x_4} \frac{x^3 + 1}{x^2} dx = \frac{x_4^2 - x_2^2}{2} - \frac{1}{x_4} + \frac{1}{x_2} \tag{15}$$

The finite part of the integral was computed for the following nodal coordinates: $x_1 = \{-1.5, -2, -3\}$, $x_2 = -1$, $x_3 = 0$, $x_4 = 1.5$, and $x_5 = \{3, 4, 6\}$, being the exact value -1.041667. The nodal coordinates produce distorted elements. Therefore, the relation between x and ξ established by the shape functions in eqns (16) and (17) is non-linear.

$$x(\xi) = \phi^1(\xi)x_1 + \phi^2(\xi)x_2 + \phi^3(\xi)x_3 \quad \text{on} \quad \Gamma^a \tag{16}$$

$$x(\xi) = \phi^1(\xi)x_3 + \phi^2(\xi)x_4 + \phi^3(\xi)x_5 \quad \text{on} \quad \Gamma^b \tag{17}$$

It should be indicated that the locations of x_1 and x_5 do not affect the value of the integral, only the transformation between x and ξ. In these cases, the finite part integral could be not invariant with respect to the transformation, and this should be considered in the computations [10]. Table 2 summarised the computed results. In all tests, the error, with respect to the exact value, was lower than 1×10^{-9}.

4 CASE STUDY

In this section, a rectangular fluid duct defined by the domain $\Omega := [0, 1.225] \times [-0.1, 0.1]$ with flat surfaces is studied. The fluid, with density $\rho = 1.225\,\text{kg/m}^3$, allows dilatational waves to propagate with a velocity of $c_f = 340\,\text{m/s}$. The boundary was defined as follows:

$$\Gamma_1 := [0, 1.225] \times [-0.1, -0.1], \Gamma_2 := [1.225, 1.225] \times [-0.1, 0.1],$$
$$\Gamma_3 := [1.225, 0] \times [0.1, 0.1], \Gamma_4 := [0, 0] \times [0.1, -0.1]. \tag{18}$$

The boundary Γ_4 was subjected to a uniform normal velocity $v_n^i = 1$ m/s, while the opposite boundary Γ_2 had a non-reflecting condition given by $p^i/v_n^i = \rho c_f$. The boundary conditions were the same as set $v_n^i = 0$ at $\Gamma_{1,3}$. The problem wavelength was defined from the duct

Table 2: Results of the test on the integration procedure.

Case	x_1	x_2	x_3	x_4	x_5	Exact value	Numerical value	Error [$\times 10^{-9}$]
1	−1.5	−1.0	0.0	1.5	3.0	1.041667	1.041667	0.218811
2	−2.0	−1.0	0.0	1.5	3.0	1.041667	1.041667	0.181570
3	−3.0	−1.0	0.0	1.5	3.0	1.041667	1.041667	0.144573
4	−1.5	−1.0	0.0	1.5	4.0	1.041667	1.041667	0.201584
5	−2.0	−1.0	0.0	1.5	4.0	1.041667	1.041667	0.164343
6	−3.0	−1.0	0.0	1.5	4.0	1.041667	1.041667	0.127347
7	−1.5	−1.0	0.0	1.5	6.0	1.041667	1.041667	0.184385
8	−2.0	−1.0	0.0	1.5	6.0	1.041667	1.041667	0.147145
9	−3.0	−1.0	0.0	1.5	6.0	1.041667	1.041667	0.110148

length ($L = 1.225\,\mathrm{m}$), being $\lambda = L/20\,\mathrm{m}$, leading to a frequency of $5551\,\mathrm{Hz}$. The model was discretised into elements with nodes located at Chebyshev points of the first kind of length h ensuring that $\kappa h = 3$, and order $p = 6$. This problem has an analytical solution for the one-dimensional case [11] that can be used for comparison purposes, given the geometry of the problem.

Fig. 3 shows a comparison between the analytical solution of the problem and the numerical result obtained using both the BEM formulation and the hypersingular one.

Once the good performance of the formulation had been verified, a straight inclusion in the duct was considered to work as a barrier. Fig. 4 schematises the geometry of the duct and inclusion. The inclusion in the duct has a small thickness equal to $10^{-4}\,\mathrm{m}$ and can therefore be considered null thickness. In this case, eqns (3) and (4) should be coupled to obtain the unknowns of the problem using the dual BEM.

Eqn (3) led to the following equation when the collocation point $\mathbf{x}^*$ belongs to the duct boundary:

$$
c(\mathbf{x}^*)u(\mathbf{x}^*) = \sum_{j=1}^{N_1} \sum_{i=0}^{p} \left[\left(\int_{\Gamma^j} \phi^i(\mathbf{x})\mathcal{G}(\mathbf{x}, \mathbf{x}^*)\,d\Gamma \right) t^i - \left(\int_{\Gamma^j} \phi^i(\mathbf{x})\mathcal{H}(\mathbf{x}, \mathbf{x}^*)\,d\Gamma \right) u^i \right] +
$$
$$
\sum_{j=1}^{N_2} \sum_{i=0}^{p} \left[\left(\int_{\Gamma^j} \phi^i(\mathbf{x})\mathcal{G}(\mathbf{x}, \mathbf{x}^*)\,d\Gamma \right) (t^{i+} + t^{i-}) - \left(\int_{\Gamma^j} \phi^i(\mathbf{x})\mathcal{H}(\mathbf{x}, \mathbf{x}^*)\,d\Gamma \right) (u^{i+} - u^{i-}) \right]
$$
$$(19)$$
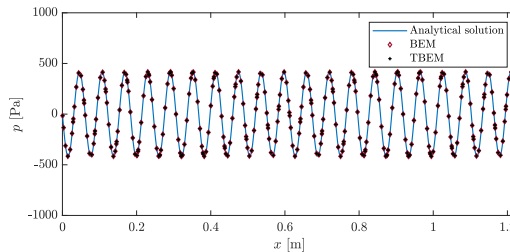
Figure 3: Analytical solution and numerical results in the middle line ($y = 0$) of a channel with height $h_d = 0.2\,\mathrm{m}$.
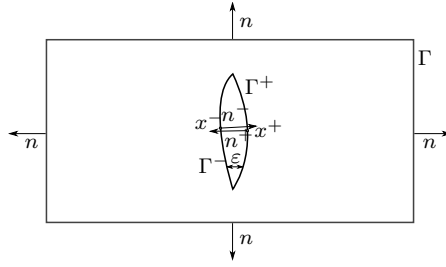
Figure 4: Geometry of the duct and inclusion ($\varepsilon \to 0$).

where N_1 and N_2 are the elements that represent the duct and inclusion with normal n^+, respectively; and u^i and t^i are related to the pressure and normal velocity, respectively.

In eqn (19), the following relations have been taken into account:

$$\int_{\Gamma^j} \phi^i(\mathbf{x}^+)\mathcal{G}(\mathbf{x}^+, \mathbf{x}^*)\, d\Gamma = \int_{\Gamma^j} \phi^i(\mathbf{x}^-)\mathcal{G}(\mathbf{x}^-, \mathbf{x}^*)\, d\Gamma \qquad (20)$$

$$\int_{\Gamma^j} \phi^i(\mathbf{x}^+)\mathcal{H}(\mathbf{x}^+, \mathbf{x}^*)\, d\Gamma = -\int_{\Gamma^j} \phi^i(\mathbf{x}^-)\mathcal{H}(\mathbf{x}^-, \mathbf{x}^*)\, d\Gamma \qquad (21)$$

corresponding to points $\mathbf{x}^+$ and $\mathbf{x}^-$ at the same barrier location but with normals n^+ and n^-, respectively.

Eqn (3) can also be applied for $\mathbf{x}^* = \mathbf{x}^+$ and $\mathbf{x}^* = \mathbf{x}^-$ leading to two equations that can be added as follows:

$$\frac{1}{2}\left(u(\mathbf{x}^+) + u(\mathbf{x}^-)\right) = \sum_{j=1}^{N_1}\sum_{i=0}^{p}\left[\left(\int_{\Gamma^j}\phi^i(\mathbf{x})\mathcal{G}(\mathbf{x}, \mathbf{x}^+)\, d\Gamma\right)t^i - \left(\int_{\Gamma^j}\phi^i(\mathbf{x})\mathcal{H}(\mathbf{x}, \mathbf{x}^+)\, d\Gamma\right)u^i\right]$$
$$+ \sum_{j=1}^{N_2}\sum_{i=0}^{p}\left[\left(\int_{\Gamma^j}\phi^i(\mathbf{x})\mathcal{G}(\mathbf{x}, \mathbf{x}^+)\, d\Gamma\right)(t^{i+} + t^{i-})\right.$$
$$\left. - \left(\int_{\Gamma^j}\phi^i(\mathbf{x})\mathcal{H}(\mathbf{x}, \mathbf{x}^+)\, d\Gamma\right)(u^{i+} - u^{i-})\right]$$

$$(22)$$

Similarly, eqn (4) allows us to obtain:

$$\frac{1}{2}\left(t(\mathbf{x}^+) - t(\mathbf{x}^-)\right) = \sum_{j=1}^{N_1}\sum_{i=0}^{p}\left[\left(\int_{\Gamma^j}\phi^i(\mathbf{x})\tilde{\mathcal{G}}(\mathbf{x}, \mathbf{x}^+)\, d\Gamma\right)t^i - \left(\int_{\Gamma^j}\phi^i(\mathbf{x})\tilde{\mathcal{H}}(\mathbf{x}, \mathbf{x}^+)\, d\Gamma\right)u^i\right]$$
$$+ \sum_{j=1}^{N_2}\sum_{i=0}^{p}\left[\left(\int_{\Gamma^j}\phi^i(\mathbf{x})\tilde{\mathcal{G}}(\mathbf{x}, \mathbf{x}^+)\, d\Gamma\right)(t^{i+} + t^{i-})\right.$$
$$\left. - \left(\int_{\Gamma^j}\phi^i(\mathbf{x})\tilde{\mathcal{H}}(\mathbf{x}, \mathbf{x}^+)\, d\Gamma\right)(u^{i+} - u^{i-})\right]$$

$$(23)$$

Eqns (19), (22) and (23) led to the dual BEM equation system that can be used to compute the pressure and the normal velocity in the duct (u^i and t^i), and at inclusion (u^{i+}, u^{i-}, t^{i+}, and t^{i-}), once the boundary conditions are imposed.

With this procedure, three problems for different-sized straight inclusions were solved. Using the geometry of the verification duct, two new coincident patches with normals in opposite directions were added in each case. Placed in the middle of the channel, the lengths of the inclusions were considered as a percentage of the height of the duct h_d: $0.3\,h_d$, $0.6\,h_d$ and $0.9\,h_d$, respectively. Thus, the two new patches implemented in each problem are as follows:

$$\Gamma_5 := [0.6125, 0.6125] \times [0.03, -0.03], \Gamma_6 := [0.6125, 0.6125] \times [-0.03, 0.03] \quad (24a)$$
$$\Gamma_5 := [0.6125, 0.6125] \times [0.06, -0.06], \Gamma_6 := [0.6125, 0.6125] \times [-0.06, 0.06] \quad (24b)$$
$$\Gamma_5 := [0.6125, 0.6125] \times [0.09, -0.09], \Gamma_6 := [0.6125, 0.6125] \times [-0.09, 0.09] \quad (24c)$$

The fluid properties, as well as the boundary conditions set in the duct, the wavenumber value, and the element discretization remained the same as in the non-barrier problem. Meanwhile, for $\Gamma_{5,6}$ the normal velocity was imposed as $v_n^i = 0$.

(a)

(b)

(c)
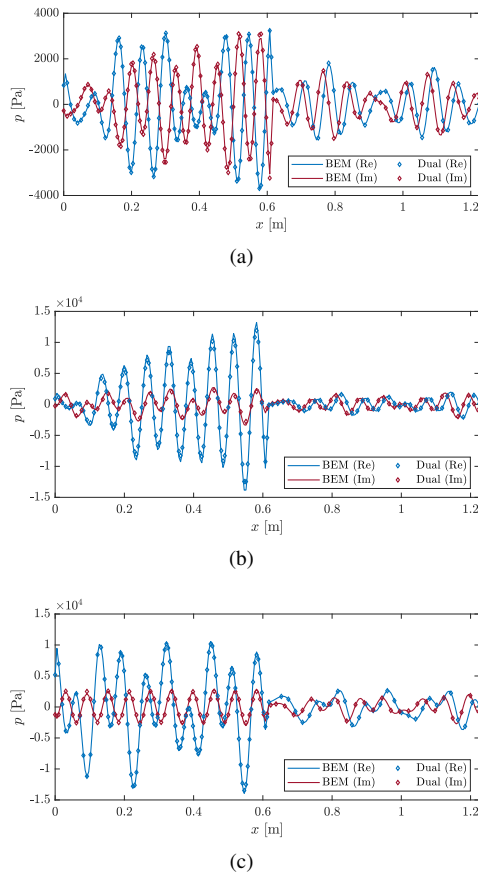
Figure 5: Pressure values for a frequency of $5551\,\mathrm{Hz}$ in the middle line ($y = 0$) of a channel of height $h_d = 0.2\,\mathrm{m}$. Comparison between the numerical results obtained with the two numerical formulations with a barrier length of: (a) $0.3\,h_d$; (b) $0.6\,h_d$; and (c) $0.9\,h_d$.

The main advantage of the proposed Dual BEM procedure lies in the possibility of easily introducing thin elements, achieving accurate results through the use of fewer patches.

Fig. 5 shows the pressure in the middle line ($y = 0$) of the three problems considered. Each graph displays a comparison between the results obtained by using the BEM formulation (solid lines) and Dual BEM formulation (markers) for both imaginary and real values. The good agreement between the curves in each case is easily noticeable, which confirms the strong performance of the proposed formulation.

5 CONCLUSIONS

This paper enhances the abilities of the QUEEN quadrature presented in Velázquez-Mata et al. [1] to solve engineering problems. First, the numerical quadrature has been extended to consider singularities of type $1/r^2$, since the original quadrature only enables computation of singularities such as $\log(r)$ and $1/r$. This novelty is highly successful, to the best of the author's knowledge, in developing BEM codes without the need for the regularisation process. Second, the novel quadrature has been used to solve the Helmholtz equation on a boundary with open geometry. The results of the classical and hypersingular BEM formulations have been shown, highlighting the capabilities of each methodology. The hypersingular BEM formulation was more accurate for computing the considered problems where Dirichlet boundary conditions were prescribed, while the classical BEM formulation was more accurate in the case of Neumann boundary conditions.

Finally, a more complex problem consisting of a rectangular duct that includes a small-thickness barrier has been analysed to show the capabilities of the quadrature in the Dual BEM formulation.

ACKNOWLEDGEMENTS

REFERENCES

[1] Velázquez-Mata, R., Romero, A., Domínguez, J., Tadeu, A. & Galvín, P., A novel high-performance quadrature rule for BEM formulations. *Engineering Analysis with Boundary Elements*, **140**, pp. 607–617, 2022.

[2] Domínguez, J., *Boundary Elements in Dynamics*. Computational Mechanics Publications and Elsevier Applied Science, 1993.

[3] Guiggiani, M., *Formulation and Numerical Treatment of Boundary Integral Equations with Hypersingular Kernels*. Computational Mechanics Publications: Southampton and Boston, 1998.

[4] Romero, A., Galvín, P., Cámara-Molina, J. & Tadeu, A., On the formulation of a BEM in the Bézier–Bernstein space for the solution of Helmholtz equation. *Applied Mathematical Modelling*, **74**, pp. 301–319, 2019.

[5] Brandaõ, M.P., Improper integrals in theoretical aerodynamics: The problem revisited. *AIAA Journal*, **25**(9), pp. 1258–1260, 1987.

[6] Carley, M., Numerical quadratures for singular and hypersingular integrals in boundary element methods. *SIAM Journal on Scientific Computing*, **29**(3), pp. 1207–1216, 2007.

[7] MATLAB, version 9.11.0.1837725 (R2021b). The MathWorks Inc.: Natick, MA, 2021.

 [8] Guiggiani, M. & Casalini, P., Direct computation of cauchy principal value integrals in advanced boundary elements. *International Journal for Numerical Methods in Engineering*, **24**(9), pp. 1711–1720, 1987.
 [9] Kaya, A.C. & Erdogan, F., On the solution of integral equations with strongly singular kernels. *Quarterly of Applied Mathematics*, **45**(1), pp. 105–122, 1987.
[10] Kutt, H.R., *On the Numerical Evaluation of Finite-Part Integrals Involving an Algebraic Singularity*. Stellenbosch University, 1975.
[11] Biermann, J., von Estorff, O., Petersen, S. & Wenterodt, C., Higher order finite and infinite elements for the solution of helmholtz problems. *Computer Methods in Applied Mechanics and Engineering*, **198**(13), pp. 1171–1188, 2009.